Available online at www.sciencedirect.com
SCIENCE DIRECT®
Applied Geochemistry 21 (2006) 859–869
Applied Geochemistry
www.elsevier.com/locate/apgeochem

Conceptual model for flow separation processes affecting waste package chemical environment, Yucca Mountain, Nevada

Drew Hall, John Walton *

Environmental Sciences Program, University of Texas at El Paso, El Paso, TX 79968, USA

Received 1 October 2004; accepted 6 February 2006
Editorial handling by M. Gascoyne
Available online 29 March 2006

Abstract

A conceptual model for the chemical evolution of near-field water chemistry in the proposed high-level nuclear waste repository at Yucca Mountain, Nevada is presented. This model considers the effects of differential solubility in flowing water that is subject to evaporation or condensation. The results of a simplified numerical implementation of the model are used to predict the aqueous chemistries produced from a variety of source waters under two bounding assumptions of separation. The model predicts that, under some conditions the most soluble ions will not always be present in solution. The more soluble ions may precipitate at different locations than ions of slightly less solubility leading to a highly complex system containing different brine compositions at different locations.

1. Introduction

Yucca Mountain is the proposed site for a geologic repository to dispose of high-level nuclear waste generated predominantly in power plants across the US Current designs call for waste packages to be emplaced in a thick layer of partially saturated tuff between the ground surface and the water table. A combination of natural and engineered components will influence radionuclide storage and mobility in the environment. Natural barriers at Yucca Mountain make up the primary system of containment; additional waste isolation performance will be obtained by employing an engineered barrier system (EBS). The major components of the EBS include: a support system to house waste bundles, stainless steel cylinders to contain the waste, an exterior cladding layer of Alloy 22 on the stainless steel cylinders that provides resistance to localized and general corrosion, and drip shields to prevent water from contacting the waste containers (OCRWM, 2001).

The performance of the EBS is influenced by the composition of the water contacting individual EBS components and, eventually, the waste. For example, localized corrosion of the Alloy 22 cladding is more likely to occur in conditions where the molar ratio of Cl^- to NO_3^- is high (Cragnolino et al., 2003; Payer et al., 2002). Water composition will also play a role in the corrosion of other EBS components and estimating the solubility of individual radionuclides.

The goal of this study is to develop an improved conceptual understanding of the evolution of hydrochemical systems within the EBS and to explore

* Corresponding author.
E-mail address: walton@utep.edu (J. Walton).

0883-2927/$ - see front matter © 2006 Elsevier Ltd. All rights reserved.
doi:10.1016/j.apgeochem.2006.02.018

some of the implications of the conceptual model. Many factors, including the partial pressure of CO_2, temperature, and oxidation–reduction conditions influence the evolution of water chemistry. This study will more closely examine the role of separation of dissolved constituents based upon differential solubility in flowing water that is subject to evaporation or condensation.

The separation of ions in water can occur by different mechanisms. The first can occur when water moves during the evaporation process, causing different minerals to precipitate at different locations based on relative differences in solubility. The second can occur when relative humidity increases with time, causing water to condense on evaporite deposits and sequentially remove the most soluble ions by dripping or flow.

2. Conceptual model

In order to have aqueous water chemistry, one must have water. Wetting of the EBS can occur in at least three ways: as drips falling from asperities in the ceiling of the drift, capillary condensation, and/or condensation promoted by dusts and hygroscopic precipitates (Simmons, 2003; Walton, 1994). During early periods following waste emplacement, when temperatures and temperature gradients are predicted to be highest, most of the water dripping or seeping into the repository will evaporate (Buscheck et al., 2002, 2003; Haukwa et al., 1999), potentially forming precipitates within the repository host rock, at the rock/air interface in drifts, and/or on EBS materials. Later in time, evaporation and condensation may occur on a smaller scale as the drifts themselves begin to collapse, which will slow heat transfer and create temperature gradients in the rubble and corrosion products even at low heat-generation rates.

Even without rock fall or backfill, spatial variability in thermal conductivity and differences in waste package heat generation can lead to localized evaporation and condensation cells (Buscheck et al., 2002). Natural ventilation occurring through the host rock, open drifts, rockfall and backfill also influences the development of these cells. For these reasons, evaporation and condensation processes cannot be easily constrained to a finite time period or location, although evaporation and condensation will slow with time as energy levels drop.

In general, liquid water is not stagnant during these evaporation and condensation processes, but instead moves in response to surface-tension-related forces and/or gravity. Consider a situation where water in the host rock evaporates into the drift. Although modeling analyses tend to assume relatively homogeneous (i.e., averaged) flow properties, rock is heterogeneous at small scales and as a result, some areas of the drift have a better connection to source waters than others. Capillary forces then result in water flow from better to more poorly connected areas. A similar process will occur when liquid water is present as a film on EBS surfaces or drift walls. Evaporation into the drift will continue as the water moves, leading to sequentially greater concentration of dissolved constituents. As the water concentrates, less soluble minerals will precipitate first at one location followed sequentially by more soluble minerals precipitating at other locations, resulting in the physical separation of the minerals.

Such a separation of dissolved constituents may occur on EBS components, surrounding drift walls, and/or in the host tuff. After precipitation, the minerals may migrate as dust or later be mobilized by condensate or infiltrating water (OCRWM, 2000a). In general, the rewetting of salts will be by deliquescence as relative humidity rises (Walton, 1994).

Evaporation occurs in many combinations of geometry and microenvironment. In Fig. 1, a small crack in the drift wall is chosen for illustration purposes. Relative humidity and temperature are assumed to vary in the crack, based upon access to the drift. Lower relative humidity near the drift leads to a capillary pressure gradient in the rock, with liquid moisture movement towards the drift. Depending upon flow and transport conditions, minerals may deposit as a homogeneous mass (see Fig. 1a) or less soluble minerals (e.g., $CaCO_3$) may precipitate near the closed end of the fracture followed by more soluble minerals near the fracture opening (e.g., $NaNO_3$) (see Fig. 1b). The minerals shown in Fig. 1 are examples based upon the following simulations.

Fig. 1 presents two mathematical models for describing potential mineral deposition: a single cell mixing tank, in which all minerals precipitate and dissolve at the same physical location (see Fig. 1a) and a multiple cell mixing tank, in which minerals may precipitate and dissolve at different locations based on differential solubility (see Fig. 1b). Multiple cell mixing tank models can be run with different numbers of cells, with the limit of infinite cells giving the maximum degree of separation anticipated by this process.

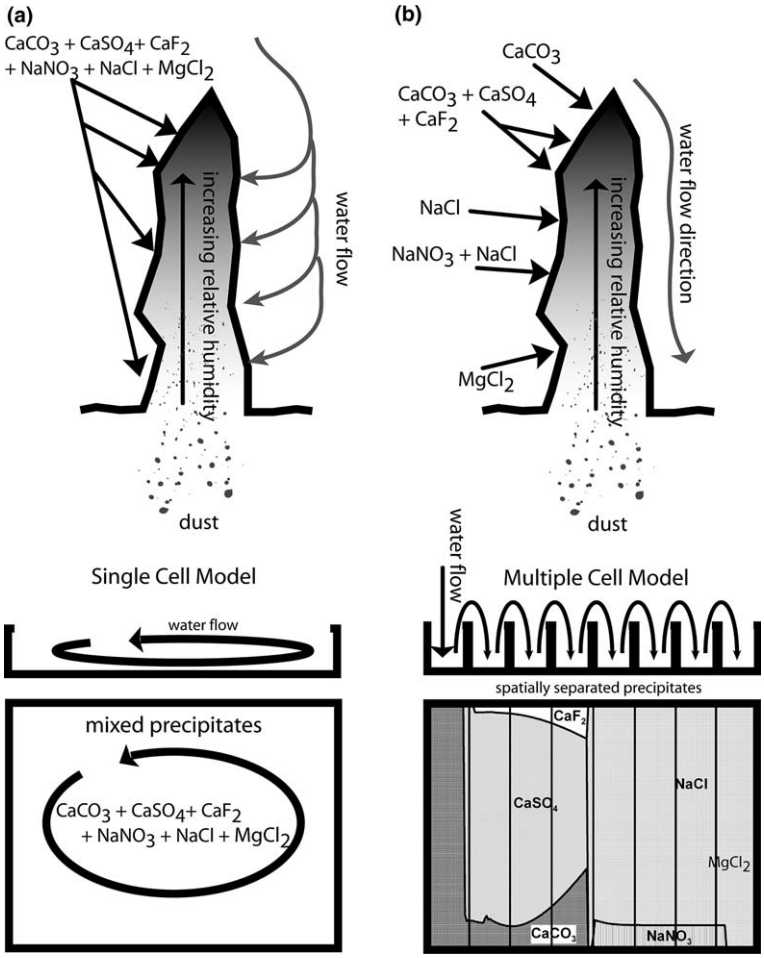

Fig. 1. Example ranges of separation of mineral precipitates in a fracture with a relative humidity gradient and corresponding mixing model with (a) no separation, and (b) significant separation.

In the multiple cell model, the source water enters the first cell as a dilute solution with a full suite of dissolved constituents. The separation occurs during a period of net evaporation, as water moves from cell to cell. Each mixing cell in the series is physically separated from the previous cell, separating each suite of minerals precipitating in each cell from those in the previous cell. Less soluble minerals are deposited preferentially near the water source and highly soluble minerals are precipitated from the more concentrated solution further from the source. Flow separation processes do not cause complete separation during mineral formation; in most situations several minerals will precipitate simultaneously from solution.

Fig. 2 illustrates the conceptual model of mineral precipitation and subsequent rehydration. The flow separation process during evaporation in the multiple cell model is illustrated in the left-most column of Fig. 2a. The environment in the multiple cell case is next presumed to pass through a period of low relative humidity, where the precipitated solids are dry, due to low relative humidity in the repository. Migration as dust or falling rock particles could occur at this time. Over time, the relative humidity of the repository as a whole, and of most individual microclimates, will increase (Haukwa et al., 1999; Buscheck et al., 2002, 2003). As relative humidity increases, the deliquescence point of the most soluble precipitates is reached first, as shown in Fig. 2a. Eventually, the deliquesence point of less soluble precipitates is reached, as illustrated in the lower right of Fig. 2a. To the right of the deliquescence point, the composition of the solution does not change, but the solution becomes more dilute as water transfers from the air into the aqueous solution.

Fig. 2b illustrates the path for the single cell mixing tank case. All minerals precipitate in a

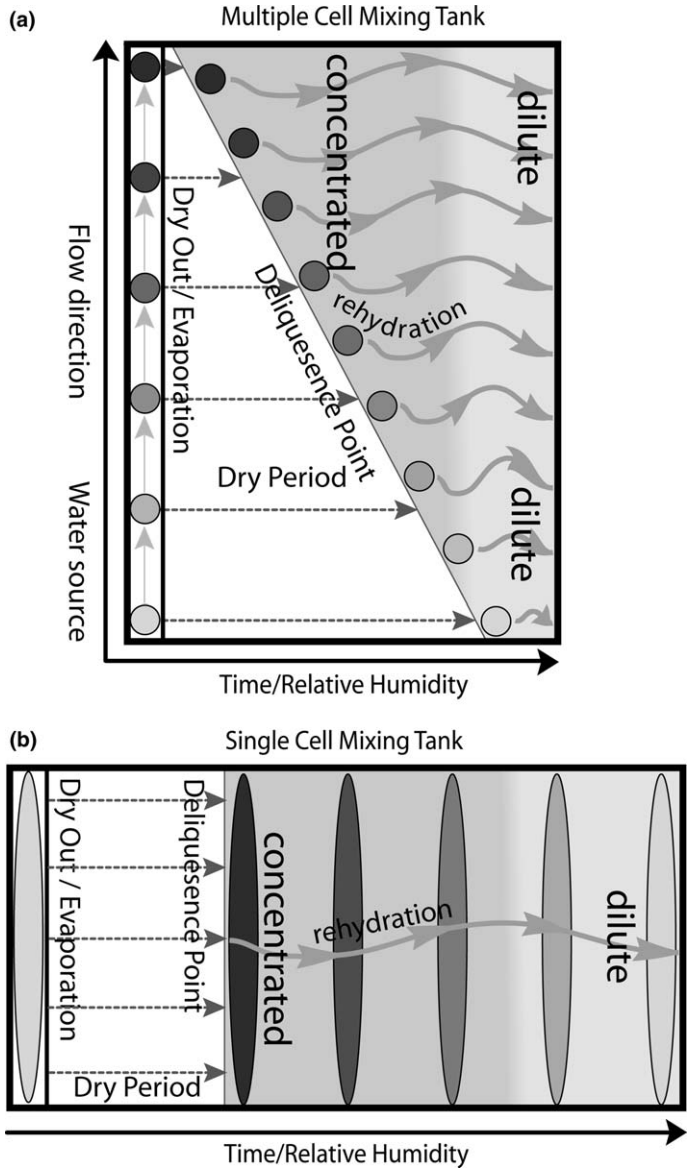

Fig. 2. Evolution of (a) multiple and (b) single cell mixing tank models.

homogeneous mass across the wetted area, shown on the left side of the figure. At a future point in time, the relative humidity of the microenvironment rises above the deliquescence point of the most soluble precipitates deposited, and an aqueous solution forms. Over time, relative humidity rises further, the composition of the solution evolves as less soluble constituents are dissolved in the increasingly dilute and heterogeneous aqueous solution. The evolution of the solution with time is the reverse of the aqueous phase evaporation sequence.

In summary, in the infinite cell case the reconstituted aqueous solution composition varies in space but not with relative humidity. In the single cell case the solution composition is constant in space but evolves with relative humidity. In the most realistic case (i.e., multiple cell mixing tank cells) the solution evolves with location and relative humidity.

Separation can also occur during the rewetting phase. Assume that a homogeneous mass of salt has precipitated at an evaporation front on the surface of the drip shield, container, or rock/air interface. As relative humidity rises, the deliquescence begins first with the most soluble salts followed by the least soluble. If gravity or capillary pressure gradients remove the water as it condenses, the aqueous

chemistry will pass through the stages of a multiple cell mixing model, with solution composition changing over time.

3. Separation conditions

The occurrence of the separation of mixed dissolved constituents has been described, but not the conditions that would promote separation. The tendency for separation is considered for two types of flow: film flow and unsaturated flow in a porous medium. Film flow can be the result of drips or water seeping down drift walls, the EBS, and/or support materials (Simmons, 2003), or deliquescence of salt deposits.

Water movement from moist to drier areas is driven by capillary pressure gradients. If ions in the water move by pure advection while evaporation occurs, concentrations will increase along the travel path and the physical separation of precipitates will be anticipated (i.e., the multiple cell case). Alternatively, the solution will concentrate as a homogeneous mass if diffusion dominates and thus smears the concentration gradient (i.e., single cell case). The ratio of advective to diffusive transport (Peclet number (Pe)) for evaporation and water movement scenarios should indicate when separation is most likely to occur.

Where water moves as a linear film, Pe is defined as

$$Pe = \text{Separation Factor} = \frac{\text{Advection}}{\text{Diffusion}} = \frac{VC}{-D\frac{dC}{dx}} \quad (1)$$

where V is velocity (m/s), C is concentration (kg/m^3), D is the diffusion coefficient (m^2/s), and x (m) is the distance from the beginning of the linear film. The expression for Pe can simplified by using the following approximate relations.

Water balance for a one-dimensional linear film can be expressed as

$$q = q_i - Ex \quad (2)$$

where q is the volumetric flow rate per unit width of the film (m^3/(m s)) at any x location, q_i is the initial volumetric flow rate per unit width of the film (m^3/(m s)), and E is evaporation per unit area of the film (m^3/(m^2 s)). E and q_i are constants whereas q is a function of x.

The maximum concentration gradient, before diffusion and/or precipitation, is given by

$$\frac{dC}{dx} \cong \frac{-C}{q_i}\frac{dq}{dx} \quad (3)$$

This is a mathematical statement that the initial concentration gradient at any point results from evaporative concentration. $d(q/q_i)/dx$ reflects the fractional loss of water from evaporation as the water flows along the film at any point. The statement is approximate because precipitation of solids is not considered. Precipitation flattens the concentration gradient, thereby slowing diffusion. This causes the derived dimensionless group to underestimate the tendency for separation. Since q_i is a constant it can be removed from the derivative. The flow velocity is given by:

$$v = \frac{q}{\delta} \quad (4)$$

where δ (m) is the film thickness.

Substituting these relations into Eq. (1) and then simplifying gives

$$Pe = \frac{q_i(q_i - Ex)}{\delta DE} \quad (5)$$

Following the same steps for a circular film with radial flow of radius r (m) and the water source (i.e., seep or drip) in the center:

$$Pe = \frac{Q_i(Q_i - E\pi r^2)}{\delta DE(2\pi r)^2} \quad (6)$$

where Q_i has units of m^3/s for a circular film.

The edge of the film for linear and radial flow, where all the water has evaporated is given by

$$(q_i - Ex) = 0 \quad (7)$$

$$(Q_i - E\pi r^2) = 0, \quad (8)$$

respectively.

Eqs. (5) and (6) are used to indicate situations where flow separation is most likely. Flow separation is predicted when the separation factor (Pe) is significantly greater than one. According to the derived equations, the separation factor is greatest at the water source area and zero at the edge of the film where it dries out, assuming sufficient area is available for the film to dry at one end. At x or $r = 0$, where maximum separation is predicted, the separation factor for linear flow simplifies to

$$Pe = \frac{q_i^2}{\delta DE} \quad (9)$$

and to infinity for radial flow.

Low input water rates produce little to no advective transport and a low separation factor across the range of evaporation. Separation is also low for very high evaporation rates over a range of input

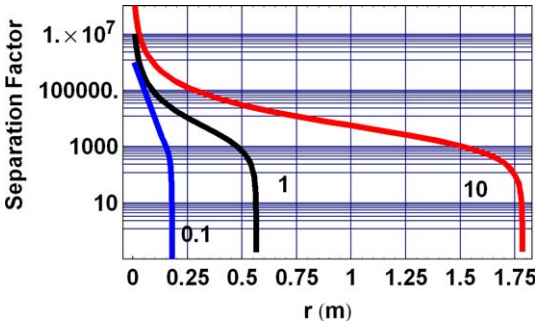

Fig. 3. Separation factor for circular film of water as a function of film radius and evaporation rate.

rates. For example, when water rapidly "flashes off" a hot surface, little separation of dissolved constituents occurs.

Fig. 3 illustrates the effect of the film radius and evaporation rate on the separation factor for a circular film. In this example D is 10^{-9} m^2/s, δ is 10^{-3} m, Q is 1 m^3/a, and E is variously 0.1, 1, and 10 m^3/(m^2 s). Each line traces the separation factor from the center of the drip location to the edge of the wetted fringe where the film has completely evaporated. The separation factor asymptotes to infinity at the center and to zero at the edge of the film. From a corrosion viewpoint the waters become potentially more aggressive as they concentrate at greater radial and linear distances. It is fortunate that flow separation declines as the water concentrates, however Fig. 3 indicates that flow separation is anticipated over most of the area of the three films shown.

For porous media, a linear flow is assumed parallel to the evaporation surface (see Fig. 1b) and a separation factor of

$$Pe = \text{Separation Factor} = \frac{VC}{-D_e\left(\frac{dC}{dx}\right)} \tag{10}$$

where D_e (ψ) is the effective diffusion coefficient expressed as a function of the capillary pressure head ψ (m^2/s). Conca and Wright (1992) have demonstrated that diffusion coefficients under partially saturated conditions depend primarily upon the volumetric water content, which is itself a function of capillary pressure.

Following the same approach for film flow, the Pe for porous media flow can be simplified using the following relations. The maximum concentration gradient for diffusion to work against is

$$\frac{dC}{dx} \cong -C\frac{d\theta}{dx} \tag{11}$$

where θ is the volumetric moisture content (m^3/m^3). This equation states that the initial concentration gradient is caused by the loss of water from evaporation. The derivative on the right side of Eq. (9) can be rewritten as:

$$\frac{d\theta}{dx} = \frac{d\theta}{d\psi}\frac{d\psi}{dx} \tag{12}$$

Substituting Darcy's Law and Eqs. (11) and (12) into Eq. (10) gives

$$Pe = \frac{K}{-D_e\left(\frac{d\theta}{d\psi}\right)} \tag{13}$$

where $K(\psi)$ is hydraulic conductivity (m/s) as a function of ψ.

In the porous media case, the evaporation rate component cancels, making the separation factor a function of only the capillary pressure head, ψ, and the constitutive properties of the porous medium (Eq. (13)). The three terms in Eq. (13): K, D_e, and $\frac{d\theta}{d\psi}$, are functions of the capillary pressure head (ψ). Permeability and Van Genuchten parameters for two different averaged sets of properties for Topopah Springs tuff rock: Tuff 1 from OCRWM (2001) and Tuff 2 from Lui and Bodvarsson (2003) were used to estimate K and $\frac{d\theta}{d\psi}$ as a function of ψ. Combining the diffusion coefficient versus water content results from Conca and Wright (1992) with the Van Genuchten relationships and parameters for Tuff 1 and Tuff 2 allowed the estimation of the separation factor for tuff rocks (see Fig. 4). Fig. 4 suggests that in both tuffs, separation is likely to occur over the entire range of capillary pressure, as long as flow is parallel to the evaporation surface.

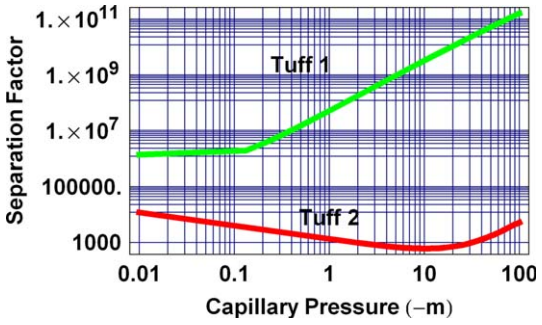

Fig. 4. Separation factor for porous media, using two different sets of unsaturated hydraulic properties for tuff rock at Yucca Mountain.

4. Numerical model description

The major steps in brine evolution during evaporation can be interpreted using the chemical divide system devised by Eugster and Hardie (1978). As the water concentrates, solute levels increase until one or more precipitates reaches saturation, and precipitates. The sequence of precipitates (i.e., chemical divides) is controlled by the sequential depletion of specific cations or anions. The chemical divide concept provides a sequence of dominant ion evolution; however it is an incomplete history of precipitates, since the normal case of simultaneous precipitation of a suite of phases is ignored.

Several relatively complex numerical models are available to predict brine evolution. Sanford and Wood (1991) used the PHRQPITZ program developed by Plummer et al. (1988). The US Department of Energy (DOE) uses the model EQ 3/6 to simulate the evaporative chemical evolution of YMP waters, also based on the Pitzer methods (OCRWM, 2000a). Given the conceptual nature of this work and the open-ended nature of the conditions described (e.g., unspecified temperature history, uncertain initial conditions) it was deemed preferable to develop and use a numerically simple model to provide a first conceptual look at potential implications. Precise predictions would require more sophisticated models, along with corresponding temperature, humidity, and flow rate estimates.

At each step in the model developed for this study, an input fraction of the remaining water is evaporated and all supersaturated minerals are precipitated. The aqueous concentrations display a history of the brine composition as it evolves and becomes more concentrated. Assuming the relative humidity at any location increases over time after the initial dryout, a reversal of the chemical evolution of the aqueous system during dryout gives the prediction for the single cell mixing tank case. For the multiple cell mixing case, each model step (i.e., the fraction of water evaporated) represents a mixing cell, and all precipitates from that model step occur in separate physical locations from other model steps. The multiple cell model results in the figures are simply a record of the precipitates formed at each evaporation step. A more in- depth explanation of the model is presented in Hall and Walton (2003).

The minerals used in the model and their solubility constants are shown in Table 1. The mineral suite is based on the analytical work presented in Rosenberg et al. (2001). These minerals are the major precipitates found from evaporation of Paintbrush non-welded tuff (PTn) pore water and well water from *J*-13, a well in Fortymile Wash, SE of Yucca Mountain. Trona was excluded from the model because its precipitation may be kinetically inhibited. Solubility constants were calculated from Gibb's free energies of formation values (Robie et al., 1978). The partial pressure of CO_2 is fixed at atmospheric. The numerical implementation of the model does not compensate for temperature.

Four possible starting water compositions are listed in Table 2. Starting water compositions were selected from Rosenberg et al. (2001), OCRWM (2000b) and Meijer (2002). Waters were selected

Table 1
Mineral precipitates considered with solubility constants

Mineral	Formula	Log of solubility constant (25 °C)
Calcite	$CaCO_3$	−9.316
Chloromagnesite	$MgCl_2$	22.01
Fluorite	CaF_2	−10.6
Gypsum	$CaSO_4$	−4.58
Halite	NaCl	1.57
Sellaite	MgF_2	−9.26
Magnesite	$MgCO_3$	−9.202
Niter	KNO_3	−0.00971
Hydrophilite	$CaCl_2$	11.92
Soda-niter	$NaNO_3$	1.094
Sylvite	KCl	0.912
Thenardite	Na_2SO_4	−0.273

Table 2
Starting water compositions by constituent

Concentration of constituents by water type (mg/L)				
Constituent	Unsaturated zone pore water		Precipitation[a]	Mixed composition
	PTn[b]	TSw[c]		50% concentrated precipitation 50% PTn[a,b]
Ca^{2+}	65.0	43.0	0.78	36.4
Mg^{2+}	12.0	3.70	0.10	6.50
K^+	0.01	N/A	0.20	1.01
Na^+	9.00	67.0	0.55	7.25
SiO_2	46.0	35.0	0.17	23.9
F^-	N/A	N/A	0.02	0.10
Cl^-	77.0	88.0	0.35	40.3
HCO_3^-	66.0	170	1.22	39.1
NO_3^-	12.0	16.0	1.55	13.8
SO_4^{2-}	79.0	19.0	0.96	44.3

[a] Meijer (2002).
[b] Rosenberg et al. (2001).
[c] OCRWM (2000b).

based on proximity to the repository and the potential to enter the repository.

Historically, *J*-13 well water has been assumed to be a convenient proxy for water in the Yucca Mountain area and is used in DOE studies of the chemical environments (Harrar et al., 1990); however, the likelihood that such water will form above the repository and affect EBS corrosion is low. It is more likely that unsaturated zone water, including pore water, pore water mixed with condensate, and pore water mixed with infiltrating waters from rain and/or snow, will contact the EBS in the future. PTn pore water is present in the horizon above the repository. Topopah Spring welded tuff (TSw) pore water exists in the repository horizon. Rainwater (i.e., precipitation), subsequent to varying degrees of interaction with pore waters and rock, also has the possibility of contacting the EBS through infiltration after large precipitation events.

5. Modeling results

The ordinate for all analyses is the fraction of the total anion composition by charge. The abscissa for the single cell mixing tank analysis is labeled as the activity of water. Given the simplicity of the numerical model, the activity of water should be interpreted as a qualitative degree of evaporative concentration. The data are displayed in this format because the activity of water roughly translates to ambient relative humidity. The amount of dissolved ions and the amount of water remaining in the solution, depends upon the initial amount of water and the initial composition of that water. For perspective, about 99.99% of the initial water is lost by the time the relative humidity reaches 90% whereas the mass precipitated from solution tends to occur predominantly in steps, which are distributed approximately evenly throughout the dryout process.

The interpretation upon rehydration is that as relative humidity rises, the precipitates begin to absorb water and the brine evolves in reverse of the evaporative sequence, becoming more like the starting water composition. The abscissa for the multiple cell mixing tank analysis is a spatial scale relative to the water source. It is much like looking at the radius of a wetted area from the side, with the water source on the left and the wetted area fringe on the right. At each location (mixing tank) the ordinate is the fraction of each anion by charge in the precipitated mass.

Fig. 5 illustrates the single cell mixing tank model results for PTn and TSw waters, precipitation water, and a mixture of PTn and precipitation water. Fig. 6 illustrates multiple cell mixing tank model results for the same water types.

PTn pore water is rich in Ca, SO_4^{2-} and Cl^-. Single cell mixing tank model results for PTn water are shown in Fig. 5a. Most of the SO_4^{2-} and HCO_3^- anions are removed from the brine during initial concentration steps as the result of the precipitation of calcite and gypsum, respectively. To graphically illustrate SO_4^{2-} and CO_3^{2-} in Fig. 5a during the initial concentration steps, it would be necessary to use a log scale for the activity of water. After these initial concentration steps, the brine composition is dominated by Cl^-, with approximately 10% NO_3^-.

The results for PTn pore water in a multiple cell mixing tank model are shown in Fig. 6a as the anion composition of the precipitated formed at each location (cell). Bicarbonate is the first anion to precipitate and is depleted by calcite formation. The middle portion of the precipitation sequence is dominated by the precipitation of SO_4^{2-} as gypsum and HCO_3^- as magnesite. Chloride precipitates beginning with halite followed by sylvite during NO_3^- precipitation, and hydrophilite at the end of the precipitation sequence. Niter and soda-niter precipitate, respectively, in small quantities relative to halite, due to the lower aqueous solubility of halite, which limits soda-niter precipitation by depleting the aqueous concentration of Na. Potassium is present in very low concentrations in PTn pore water, which limits the mass of niter that can precipitate. The resulting precipitates form an area at the end of the evaporation sequence that is predominantly Cl^-. Upon rehydration, this area in particular may present an increased localized corrosion risk, because there is little NO_3^- or SO_4^{2-} present to mitigate the effects of Cl^-. It should be noted that minor amounts of all initial source anions are predicted to be present on the right hand side of Fig. 5a and Fig. 6a, and all the other single and multiple cell models, but appear only on a log scale ordinate.

TSw pore water is HCO_3^-, Na, and Cl^- rich. The TSw geologic unit will contain the repository (Struckless and Dudley, 2002). The single cell mixing tank model (see Fig. 5b) produces brine dominated by NO_3^- and Cl^-. Separation under the multiple cell mixing tank model presents a different brine composition upon rehydration (see Fig. 6b). Bicarbonate is removed first in the form of calcite and magnesite. Sulfate precipitation follows in the intermediate stage of concentration where it precipitates as thenardite and small amounts of gypsum. Gypsum precipitation

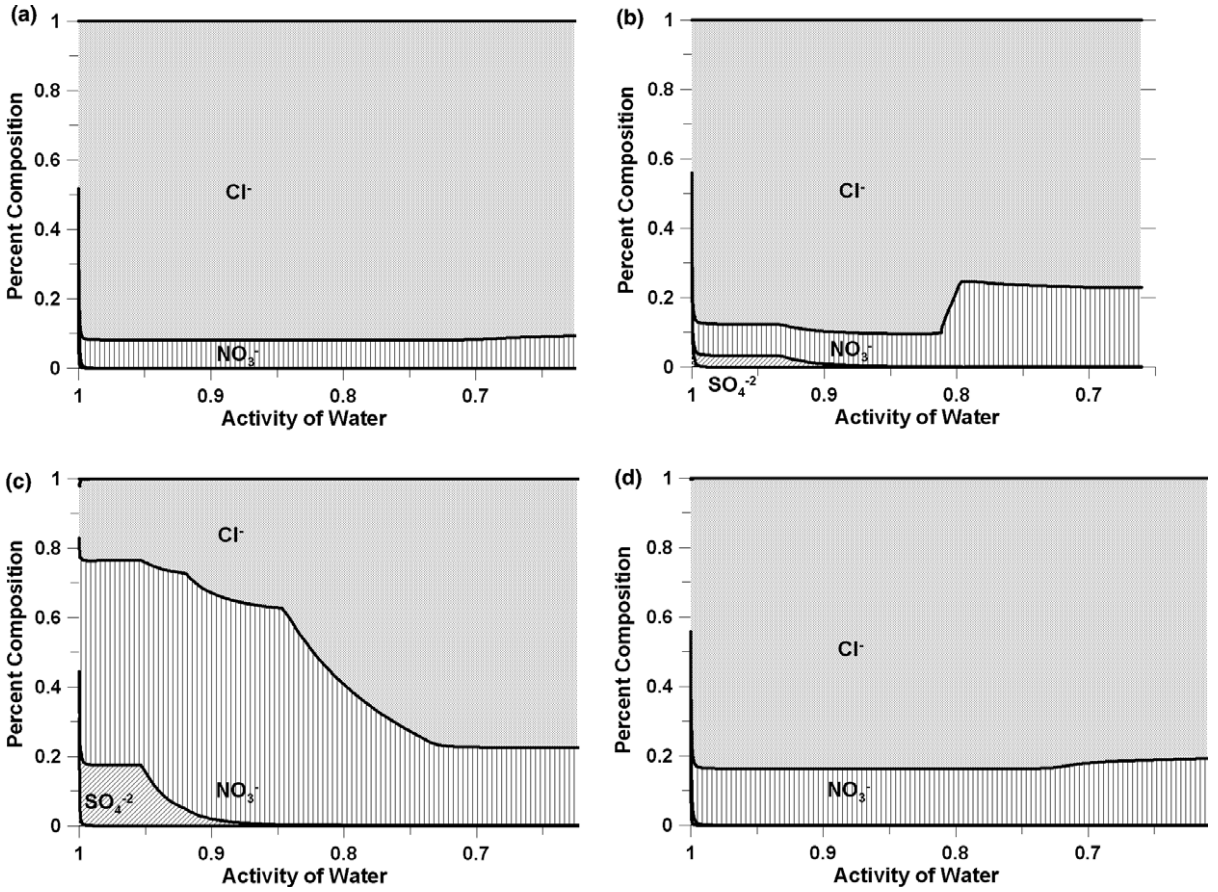

Fig. 5. Single cell mixing tank model results for four types of starting water. (a) PTn pore water. (b) TSw pore water. (c) Precipitation water. (d) Mixture of PTn and precipitation water.

is limited by low aqueous concentrations of Ca. Chloride precipitates as halite just before NO_3^- precipitates as soda-niter, due to the higher solubility of soda-niter. The band of nearly pure halite contains most of the Cl^- mass. This band is of particular interest because Cl^- in this location is spatially separated from NO_3^-. Upon rehydration, the band of pure halite is potentially corrosive. Halite and soda-niter precipitate near the wetted area fringe.

Precipitation water (i.e., rainwater) could be an important component of the water contacting the EBS after the thermal pulse. The single cell mixing tank results (see Fig. 5c) begin with dominant and nearly equal concentrations of NO_3^-, HCO_3^- and SO_4^{2-}, and lesser amounts of Cl. Again, HCO_3^- is quickly removed from solution as calcite and magnesite (the abscissa scale does not show its presence). The next change in the brine is the removal of SO_4^{2-} through gypsum and thenardite precipitation. Large amounts of Na in solution at this stage of evaporation allow for much of the NO_3^- to precipitate as soda-niter, with some halite.

The multiple cell mixing tank model results for precipitation water are complex in terms of banding and physical separation of precipitates (see Fig. 6c). Initially, HCO_3^- is precipitated as calcite and magnesite, and F^- is precipitated as fluorite. Sulfate then precipitates, forming gypsum and thenardite. Gypsum and thenardite formation decline in an area near the middle of the separation sequence, where the precipitation of F^- (i.e., fluorite) and HCO_3^- (i.e., magnesite) increase. Nitrate then forms a band of niter and soda-niter. Low concentrations of K limit the amount of niter that can form, but soda-niter precipitation is relatively unrestricted. Chloride precipitates first as halite, followed by sylvite near the end of the precipitation sequence.

Mixing and matrix diffusion processes could result in a water chemistry intermediate between precipitation and pore water. A mixture of 50% PTn

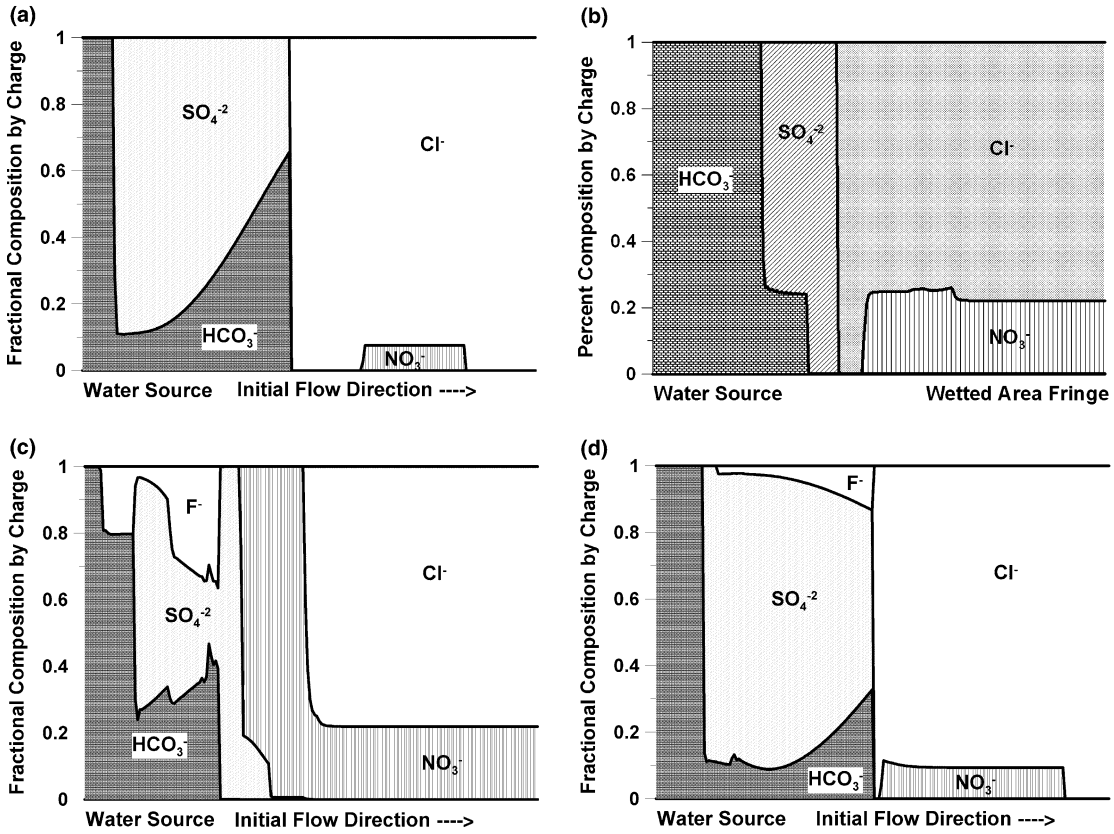

Fig. 6. Multiple cell mixing tank model results for four types of starting water. (a) PTn pore water. (b) TSw pore water. (c) Precipitation water. (d) Mixture of PTn and precipitation water.

pore water with 10 times concentrated precipitation water is used. The single cell mixing tank model results for this mixed water are different from both PTn pore water and precipitation water, despite the relatively small contribution precipitation water makes to the overall chemistry. In addition to the higher concentrations of NO_3^- and lower concentrations of Cl^- in the mixed water compared to PTn water, a number of precipitates form in the early concentration steps of the mixed water that are not found in the other waters. The evaporation sequence begins with HCO_3^- removal through calcite precipitation (see Fig. 5d). Calcium in this water is not as limiting as it is in most other cases shown previously. Fluoride cannot be seen in Fig. 5d because of its low concentrations relative to other anions, but there is a small amount of F^- present, which precipitates as fluorite. Since Ca is not limiting, fluorite precipitates, and F^- is removed from solution just as SO_4^{2-} begins to precipitate at the beginning of the evaporation sequence. Through most brine evolution, Cl^- and NO_3^- are the dominant anions in the brine.

The precipitation sequence for the mixed water in the multiple cell mixing tank model is presented in Fig. 6d. Bicarbonate is precipitated as calcite near the water source. Sulfate and F^- then precipitate as gypsum and fluorite, respectively. As gypsum precipitation declines, HCO_3^- precipitates as magnesite. Last to precipitate is Cl^- as halite, followed by sylvite and a thin band of pure hydrophilite. Niter and soda-niter precipitate during halite and sylvite formation. Upon rehydration, the band of pure hydrophilite is potentially corrosive to EBS metals.

6. Conclusions

Waste emplacement at the proposed Yucca Mountain repository will provide the energy to create macro- and micro-scale evaporation and condensation cells. These cells may significantly alter the natural hydrochemical environment within the repository and host material. Anthropogenic alteration of the hydrochemical environment may produce source waters and thermodynamic conditions

that do not currently exist. Understanding the potential impact that an altered natural environment will have on water chemistry, in this case differential solubility leading to separation of ions, will increase confidence in testing and performance assessment.

This work suggests that flow-related separation processes are likely to be active at Yucca Mountain and lead to microenvironments with water chemistry significantly different from current projections. In particular, aggressive and beneficial anions for corrosion are likely to be separated under some sets of conditions. These findings are not sensitive to choice of source water, based upon the simulations shown. More generally, current performance assessments describe averaged, large-scale, bulk conditions anticipated at the Yucca Mountain repository (OCRWM, 2000a), but neglect small-scale variations. Heterogeneities at a small scale are likely to play an important role in creating hydrochemical environments that differ substantially from averaged values. Placing uncertainty bounds on averaged values, the current approach (OCRWM, 2001), does not necessarily account for changes in water chemistry caused by small-scale phenomena and separation processes. More precise information could be obtained through full implementation of this conceptual model, with more sophisticated numerical codes and/or experiments combined with statistical analyses of probabilities of occurrence.

Acknowledgements

This work was funded by the Nye County, Nevada, Department of Natural Resources and Federal Facilities through cooperative research Grant DE-FC28-02RW12163 from the US Department of Energy, Office of Civilian Radioactive Waste Management.

References

Buscheck, T.A., Rosenberg, N.D., Gansemer, J., Sun, Y., 2002. Thermohydrologic behavior at an underground nuclear waste repository. Water Resour. Res. 38 (3), 1028.

Buscheck, T.A., Rosenberg, N.D., Blink, J.A., Sun, Y., Gansemer, J., 2003. Analysis of thermohydrologic behavior for above-boiling and below-boiling point thermal-operating modes for a repository at Yucca Mountain. J. Contam. Hydrol. 62/63, 441–457.

Conca, J.L., Wright, J.V., 1992. Diffusion and flow in unsaturated gravel, soil, and whole rock. Appl. Hydrogeol. 1, 5–24.

Cragnolino, G.S., Dunn, D.S., Brossia, C.S., Pan, Y.M., Pensado, O., Yang, L., 2003. Corrosional behavior of waste package and drip shield materials. In: 10th International High Level Radioactive Waste Management Conference, Am. Nucl. Soc., Las Vegas, NV.

Eugster, H.P., Hardie, L.A., 1978. Lakes: chemistry, geology, physicsSaline Lakes. Springer-Verlag, New York.

Hall, D.W., Walton J.C., 2003. Physical separation processes and EBS water chemistry – a modeling study. In: 10th International High Level Radioactive Waste Management Conference, Am. Nucl. Soc., Las Vegas, NV.

Harrar, J., Carley, J.F., Isherwood, W.F., Raber, E., 1990. Report to the committee to review the use of J13 well water in Nevada nuclear waste storage investigations. UCRL-ID-21867, Lawrence Livermore National Laboratories, Livermore, CA.

Haukwa, C.B., Wu, Y.S., Bodvarsson, G.S., 1999. Thermal loading studies using the Yucca Mountain unsaturated zone model. J. Hydrol. 38, 217–255.

Lui, H.H., Bodvarsson, G.S., 2003. Upscaling of constitutive relations in saturated heterogeneous tuff matrix. J. Contam. Hydrol. 276, 198–209.

Meijer, A., 2002. Conceptual model of the controls on natural water chemistry at Yucca Mountain, Nevada. Appl. Geochem. 17, 793–806.

Office of Civilian Radioactive Waste Management (OCRWM), 2000a. Engineered Barrier System: Physical and Chemical Environment Model. ANL-EBS-MD-000033 Rev. 00., Las Vegas, NV.

Office of Civilian Radioactive Waste Management (OCRWM), 2000b. Analysis of geochemical Data for the unsaturated Zone. ANL-NBS-HS-000017 Rev. 00., Las Vegas, NV.

Office of Civilian Radioactive Waste Management (OCRWM), 2001.Yucca Mountain Science and Engineering Report. DOE/RW-0539, Las Vegas, NV.

Payer, J.H., Latanision, R.M., Kelly, R.G., Jones, R.H., Frankel, G.S., Devine, T.M. Jr., Beavers, J.A., 2002. Final report, Waste Package Materials Performance Peer Review Panel. Las Vegas, NV.

Plummer, L.N., Parkhurst, D.L., Flemming, G.W., Dunkle, S.A., 1988. A computer program incorporating Pitzer's equations for calculation of geochemical reactions in brines, US Geological Survey of Water Resource Investigation Report, 88-4153.

Robie, R.A., Hemmingway, B.S., Fisher, J.R., 1978. Thermodynamic Properties of Minerals and Related Substances at 298.15 K and at Higher Temperatures. US Government Printing Office, Washington, DC.

Rosenberg, N.D., Gdowski, G.E., Knauss, K.D., 2001. Evaporative chemical evolution of natural waters at Yucca Mountain, Nevada. Appl. Geochem. 16, 1231–1240.

Sanford, W., Wood, W., 1991. Brine evolution and mineral deposition in hydrologically open evaporite basins. Am. J. Sci. 291, 687–710.

Simmons, A.M., 2003. Application of natural analogues in the Yucca Mountain Project – overview. In: 10th International High Level Radioactive Waste Management Conference, Am. Nucl. Soc., Las Vegas, NV.

Struckless, J.S., Dudley, W.W., 2002. The geohydrologic setting of Yucca Mountain, Nevada. Appl. Geochem. 17, 659–682.

Walton, J.C., 1994. Influence of evaporation on waste package and radionuclide release from a tuff repository. Water Resour. Res. 30, 3479–3487.